Design and Characterization of a Coaxial Plasma Railgun for Jet Collision Experiments

Mathew R. Coleman

Thesis submitted to the Faculty of the

Virginia Polytechnic Institute and State University

in partial fulfillment of the requirements for the degree of

Master of Science

in

Mechanical Engineering

Colin S. Adams, Co-chair

Mark A. Pierson, Co-chair

Joseph W. Meadows

February 3, 2021

Blacksburg, Virginia

Keywords: coaxial plasma gun, plasma-jet, plasma dynamics

Design and Characterization of a Coaxial Plasma Railgun for Jet Collision Experiments

Mathew R. Coleman

(ABSTRACT)

Plasma railguns are electromagnetic accelerators used to produce controlled high velocity plasma jets. This thesis discusses the design and characterization of a small coaxial plasma railgun intended to accelerate argon-helium plasma jets. The railgun will be used for the study of plasma shocks in jet collisions. The railgun is mounted on a KF-40 vacuum port and operated using a 90 kA, 11 kV LC pulse forming network. Existing knowledge of coaxial railgun plasma instabilities and material interactions at vacuum and plasma interfaces are applied to the design. The design of individual gun components is detailed. Jet velocity and density are characterized by analyzing diagnostic data collected from a Rogowski coil, interferometer, and photodiode. Peak line-integrated electron number densities of approximately 8×10^{15} cm^{-2} and jet velocities of tens of km/s are inferred from the data recorded from ten experimental pulses.

Design and Characterization of a Coaxial Plasma Railgun for Jet Collision Experiments

Mathew R. Coleman

(GENERAL AUDIENCE ABSTRACT)

Plasma is a gaseous state of matter which is electrically conductive and interacts with electric and magnetic fields. Plasmas are used in many everyday objects such as fluorescent lights, but some of the physics of plasmas are still not entirely understood. One set of plasma interactions that have not been fully explored are those which occur during high-velocity collisions between plasmas. Experiments aimed to further the understanding of these interactions require the generation of plasmas with specified properties at very high velocities.

A device known as a plasma railgun can be used to produce plasmas which meet these experimental demands. In a plasma railgun, a short pulse of current is passed through a plasma located between two parallel electrodes, or "rails". This current generates a magnetic field which propels the plasma forward. The plasma is accelerated until it leaves the muzzle of the railgun. In coaxial plasma railguns, the electrodes are concentric.

This paper discusses the design and testing of a small, relatively low power coaxial plasma railgun. Specific elements of the design are examined and the inherent physical and material difficulties of a coaxial design are explored. The experiment which was performed to confirm the properties of the plasma jets produced by the coaxial plasma railgun is explained. The results of this experiment confirm that the design succeeds in producing plasmas which meet targets for plasma properties.

Dedication

To my family for always supporting me, even from across the country during a pandemic.

Acknowledgments

No one is an island, and no thesis is completed alone. The completion of this thesis relied upon the support of many people beyond myself.

I would first like to thank my advisors Dr. Colin Adams and Dr. Mark Pierson. My path to this point has not been the smoothest, and they have patiently been with me the whole way. Their willingness to point me in the right direction when I erred has saved me many times. Thank you also to my committee member Dr. Joseph Meadows for putting up with many false starts.

Thank you to Ameer Mohammed for freely providing his extensive experience with plasma railguns and his support during testing. To my lab partners and fellow research group members, Daniel Weber and Trenton Brewer for their willingness to help me with testing even through the night, and their ability to stay lighthearted through a very difficult year. I also thank all the other graduate students who helped me with a myriad of problems, of which there are too many to list here. 2020 would have been a lot worse without all of your support.

I would also like to thank Randall Monk at the APPL, and Phil Long and Casey Lucas at the Mechanical Engineering Machine Shop for their fantastic machining work. I would like to state my appreciation as well for John Burleson's help with diagnosing electrical issues and his ability to distract me from my frustration with them.

Finally, I would like to thank my family for their support and patience.

Contents

List of Figures

List of Tables

Chapter 1

Introduction

Experimental work in plasma science requires the generation of plasma with properties specific to the task at hand. This can be difficult for certain categories of plasmas. The study of the collisional dynamics of plasma jets is a field which requires the generation of plasmas which consistently reach velocities in the tens or hundreds of kilometers per second. Devices which can achieve this are often very large and have enormous power outputs. The results are devices that are also very expensive.

For smaller-scale academic research labs, the funding and space for such large-scale plasma sources may not be available. Fortunately there are a variety of methods which can produce the required plasmas on a smaller scale as long as some compromises are acceptable. One type of scaleable apparatus used for this purpose is the plasma railgun. Plasma railguns use electromagnetic forces to accelerate plasma between two electrode "rails". Plasma railguns come in two types: coaxial, and linear or parallel-plate. Coaxial and linear guns produce differently shaped jets and perform differently in other ways. A coaxial plasma railgun, also known as a coaxial plasma gun, will open up the ability of the Virginia Tech Center for Space Science and Engineering Research to perform high-velocity jet collision experiments with a different device from the preexisting linear plasma railgun, and enable collisional studies of stagnated coaxial gun jets.

This thesis describes the design and characterization of a compact coaxial plasma railgun. The design aims to be economical, modular, and portable: capable of operating through a standard KF-40 vacuum port. The ultimate object is to construct the design and perform

a preliminary characterization of the jets produced. The following chapters discuss the necessary background knowledge on coaxial guns, design decisions, the results of preliminary characterization efforts, and the conclusions which can be drawn from them.

Chapter 2

Background

2.1 Early developement

Following the initial development of fission weapons during the Second World War, nuclear technology advanced rapidly. Not only fission, but fusion began to be seen as a useful and attainable technology. An artificial fusion reaction was used to boost the yield of a fission weapon during the *Operation Greenhouse* testing of May 1951. In November of 1952, less than ten years after the first self-sustaining artificial fission in a squash court at the University of Chicago, an artificial fusion chain reaction produced petajoules of explosive yield by a thermonuclear device during the *Ivy Mike* test[1][2].

Military applications of nuclear fusion were readily apparent, but many physicists and engineers saw great prospects in its use for civilian purposes. The United States was encouraging energy production and other uses of nuclear technology, as exemplified by President Dwight Eisenhower's 1953 "Atoms for Peace" speech to the United Nations General Assembly[3]. Scientists in the emerging field of fusion research sought to be included in this technological effort. The scientific community saw the potential of nuclear fusion to provide nearly limitless power while producing little of the waste associated with fission. However, it turned out that achieving a controlled, sustainable fusion reaction was significantly more difficult than expected. Through the 1950s, scientists around the world attempted to create fusion reactors, mostly using pinch designs[4]. By 1958, fusion research was considered important enough to include in the *Second United Nations International Conference on the Peaceful*

Uses of Atomic Energy, or the Second UNICPUAE, in Geneva, Switzerland[5].

Also known as the "Atoms for Peace" conference after Eisenhower's speech, the *First United Nations International Conference on the Peaceful Uses of Atomic Energy* had been the largest scientific conference ever conducted, and had seen the release of a significant amount of previously classified information about fission technology. The Second UNICPUAE would be even larger. With nearly 5000 attending scientists and an equal number of reporters, diplomats, industry observers, and curious onlookers, the conference would be the largest scientific gathering that had ever taken place. So many attendees were present that Geneva and other nearby towns ran out of hotel rooms[6][7]. At the conference, a massive amount of fusion-related research was released to the public. The West learned about Soviet experiments with tokamaks, and the Soviets learned of American stellarators. Many scientists brought their devices with them, some staying in Geneva for months before the conference to ensure that they would work when demonstrated to the public[8]. Although it was reported too late to be formally included in the conference, the Scylla I θ-pinch had demonstrated the first controlled thermonuclear fusion during a test at the Los Alamos Scientific Laboratory[4]. It looked like fusion power was just around the corner with only a few stumbling blocks remaining. One of these was the problem of injecting plasma into the large magnetic fields required for plasma confinement.

A solution to this problem was forthcoming at the conference. In two separate submissions in the session *Theoretical and Experimental Aspects of Controlled Fusion*, the plasma physicists Hannes Alfvén and John Marshall both proposed that magnetized concentric electrodes be used to inject plasma rings into a magnetically confined reactor chamber[9][10]. Marshall later referred to the device as a "hydromagnetic plasma gun", while Alfvén instead called it a "coaxial plasma gun". Alfvén's name would stick better than Marshall's, but they would come to be referred to by many other names as well. These suggestions were just two of the over two thousand papers submitted to the conference, and most scientists moved on.

Alfvén and Marshall began working on their designs immediately following the Geneva Conference. Over the next two years their work began to diverge. Alfvén stuck with his initial proposal, using magnetic fields to form the plasma ejected by the gun into a torus shape while feeding gas into the system continuously. Meanwhile, Marshall dropped the external magnets and allowed the plasma to exit the gun as a jet. Due to previous work in which he developed a fast-acting mechanical valve, Marshall was able to cut off gas supply once the space between the electrodes had been filled with gas[11][10]. In 1959, Marshall applied for a patent for this system and in 1960 the results of their first experiments were published[12][13]. Alfvén soon shifted his focus to the fields of astronomy and cosmology. Other scientists would continue to build upon his magnetized gun idea, but Marshall's unmagnetized gun was favored as it more conveniently solved the injection problem.

2.2 Theory and operation

2.2.1 Marshall-type guns

The most basic version of a Marshall-type coaxial plasma gun is that of two concentric electrodes. Gas is injected between the electrodes into one end of the the gun, referred to as the breech. A potential difference is applied between the two electrodes, electrical breakdown of the gas occurs, and some of the gas is ionized into a plasma. As the current flows through the plasma from one electrode to the other, a magnetic field is induced behind the plasma. The Lorentz force then causes the arc to accelerate down the barrel of the gun. Once the plasma exits the gun, the circuit is broken, the induced magnetic field dissipates, and the plasma continues moving at its final exit velocity[11].

Throughout the early 1960s, researchers used coaxial plasma guns to inject plasma into various containment schemes. The possibilities of fusion still seemed wide open, and scientists had not yet discovered which devices would be effective. Coaxial guns were used

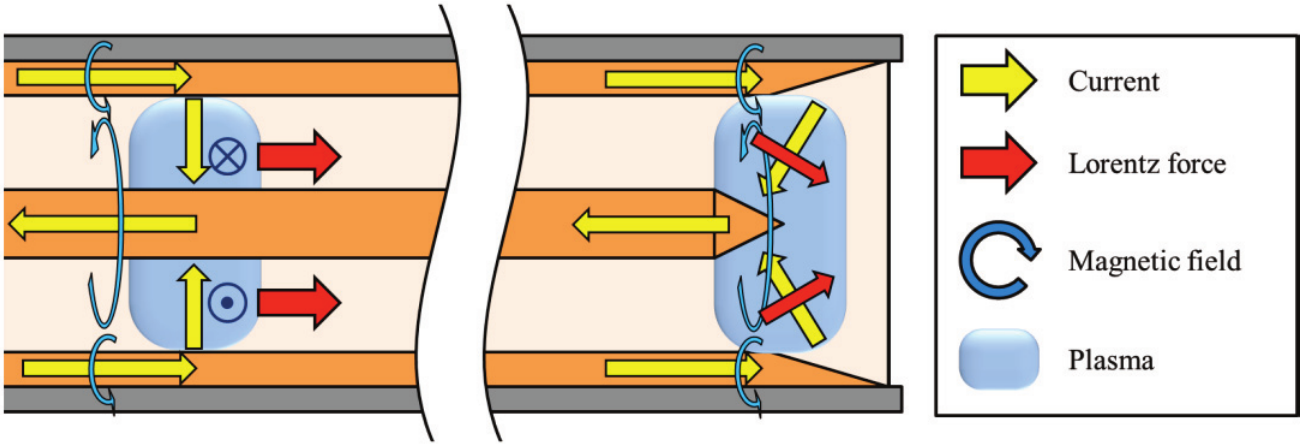

Figure 2.1: Schematic of the operation of a coaxial gun. The diagram should be understood as axially symmetric [14].

to inject plasma into cusps[15], magnetic mirrors[16], pinches[17], and shock tubes[18]. As they were using coaxial guns for their experiments, scientists also began to acquire a better understanding of the fundamental physics of their operation. John Marshall used the "slug" model, which assumes that all ionized gas, and only ionized gas, accelerates out of the gun. This simplistic approach was not true for the coaxial gun, as successive current pulses following the first would eject more plasma even when new gas was not injected into the breech[19]. It was clear that a new theoretical approach was necessary. Scientists quickly adapted the so-called "snowplow" model for use in coaxial guns. This simple model was proposed for use in pinches by M. N. Rosenbluth in 1954[20]. While some modifications have been proposed[21], the general form of the model has stayed the same since then.

For an unmagnetized coaxial gun, the snowplow model assumes that after breakdown, the current propagates as an annular sheet from one electrode to the other. This sheet "sweeps up" neutral gas as it travels down the length of the gun. Thus, mass is accumulated according to the velocity of the sheet. There is assumed to be no magnetic field in front of the current sheet. The magnetic force on the current sheet can be written as a function of the current through the sheet and the inductance per unit length of the sheet between the electrodes.

If the voltage and capacitance of the capacitor bank used to produce the current pulse are known, then a system of differential equations can be written to represent the dynamics of the system. Modified versions of the snowplow model allow for some neutral gas to avoid being swept up, as well as some current loss[22][21][19].

As coaxial plasma guns became more common, they began being applied in more novel ways. While investigating alternative acceleration modes of coaxial guns in 1965, J. W. Mather independently recreated a dense plasma focus similar to that created by N. V. Filippov in the 1950s during Soviet work on pinches[23]. Mather's design was very similar to a typical coaxial gun, but he operated it at much higher pressures. Breakdown is instantiated in the gun, and the current sheet travels down the bore in a similar way to other coaxial guns. Differences begin to occur after the sheet passes through the end of the gun, when the plasma sheet constricts into a tight, dense cylinder at the end of the inner electrode. Dense plasma focuses have been investigated for fusion power generation, and neutron and x-ray production[24][25].

2.2.2 Cheng-type guns

Publication on coaxial guns slowed in the mid-1960s, but some plasma researchers remained interested. Dah Yu Cheng, a professor at the University of Santa Clara, focused his work on a second functional mode of coaxial guns: the deflagration mode. Cheng sought to use this mode of acceleration to generate high energy, high density plasmas. In the deflagration mode, a deflagration wave moves through the plasma opposite the acceleration direction of the particles. Instead of prefilling his coaxial gun, Cheng puffed a small amount of gas into the bore. This puff was ionized and then accelerated down the gun due to $J \times B$ forces. Using this design, Cheng achieved exit velocities which were orders of magnitude higher than guns operating in the snowplow mode[26]. These high velocities gave coaxial guns promise as a method of space propulsion, which was the primary focus of coaxial gun examination

throughout the 1970s[27].

2.3 Applications

2.3.1 Spheromaks and other compact toroids

Research into magnetized guns picked up in the 1980s. Magnetized coaxial plasma guns can be used to generate stable compact plasma toroids for nuclear fusion research. There are two types of compact toroid plasmas: field-reversed configuration (FRC), and spheromak. Spheromak toroids have a toroidal magnetic field, while FRC toroids do not. Spheromaks have been of primary interest with regard to coaxial guns. To generate spheromaks using a coaxial gun, a solenoidal electromagnet is typically placed within the inner electrode, which is hollow in this layout. The magnetic field lines which pass through the bore of the gun from this electromagnet are approximately perpendicular to the direction of acceleration of the plasma within the gun. As the plasma passes through the field, it drags some of the field along with it. At the muzzle of the gun, the field deforms and then separates. This provides a torus-shaped magnetic field to the plasma, which contains it. Spheromaks can maintain stability and confinement for significant lengths of time, which gives them promise as fuel injection methods for future fusion reactors[28][29].

2.3.2 Z-pinches

In the 21st century, coaxial plasma guns have been used to generate relatively stable Z-pinches. Using a coaxial gun, plasma is accelerated in a "quasi-steady-state" into an assembly region. This quasi-steady-state is achieved by applying a very long current pulse to a puff of gas. As long as the current pulse decay is longer than the time it takes for plasma to exit the muzzle of the gun, a quasi-steady flow can be established[30]. As there are several instabilities

associated with Z-pinches, different approaches have been taken to avoid them. Shumlak et al. have used sheared flow within the z-pinch to introduce stability[31]. This method has been shown to be effective experimentally as well as theoretically[32], and has successfully produced neutrons[33]. A different approach implodes a thin shell of non-hydrogen plasma onto the pinch to suppress the instabilities. In these designs, coaxial guns can be used to generate the z-pinch[34], or to inject the shell plasma[35].

2.4 Instabilities

2.4.1 Restrike

A major source of velocity losses in plasma railguns and plasma armature railguns is secondary arcing, also known as restrike. While primarily examined in linear railguns, the effect is also present in coaxial guns. Restrike occurs when residual fields in the neutral gas not swept up by the initial current sheet cause a secondary electrical breakdown behind the primary arc. Breakdown commonly occurs at the breech due to higher gas pressure, lower velocity, and geometric irregularities caused by electrode erosion. Ablated particles from the primary arc increase the ionization of the neutral gas and make breakdown more likely. This new arc "leaches" current from the primary arc, causing a decrease in acceleration. In some cases, up to 50% of the primary arc current is lost[36]. Ablated material caught behind the primary arc increases the mass of the neutral gas, and the current within the restrike arc is not sufficient to accelerate this mass to a velocity which can reach the primary arc and combine with it. This can be thought of as a viscous drag source. Secondary arcs may be formed by several different physical phenomena, and there is no single way to prevent restrike. Restrike is extremely undesireable because it causes the primary arc to lose velocity, while the secondary arc does not reach the desired velocity either. Most research into restrike has been done for plasma armature or linear plasma railguns as the decreased ablation rates

in coaxial plasma guns reduce the incidence of secondary arcing. The simplest approaches to reducing restrike are to decrease driving current and voltage across the plasma. This decreases the ablation rate of insulators and electrodes. Low-ablation materials should also be chosen for this reason[37][38][39][40].

2.4.2 Blow-by

Radial differences in plasma exit velocity from coaxial guns were known as early as the 1960s[41], and their identification with plasma instabilities was examined to some extent[42], but a true understanding of the consequences would not occur until the 1980s. Magnetic pressure in a coaxial gun varies with the inverse square of radius. Thus, the magnetic pressure is higher closer to the center electrode, and plasma particles located there accelerate faster. As the inside of the current sheet begins to pass the outside, it may separate from the wall and compress the rest of the sheet against the outer electrode. This results in a very small part of the plasma mass accelerating to an extremely high velocity, "blowing-by" the rest of the plasma, which is compressed against the outer wall and exits much more slowly. Figure 2.2 illustrates this process. In many cases, it is desirable for all plasma to exit the gun at similar velocities, and for this to happen blow-by must be avoided. As most of the plasma near the inner electrodes separates from the wall, current must flow at high concentrations through the remaining attached plasma. In addition, this remaining plasma experiences high skin drag as it accelerates. These two combined factors cause an increased erosion of the inner electrode. The outer electrode also sustains increased erosion as the larger mass of plasma is heated due to compression while it slowly travels down the bore. Longer times spent inside the gun cause increased conduction and radiation into the outer electrode, and thus increased melting and ablation. Blow-by occurs in both magnetized and unmagnetized guns[43][44][45].

As blow-by is a consequence of the magnetic pressure inside the coaxial gun, avoiding it

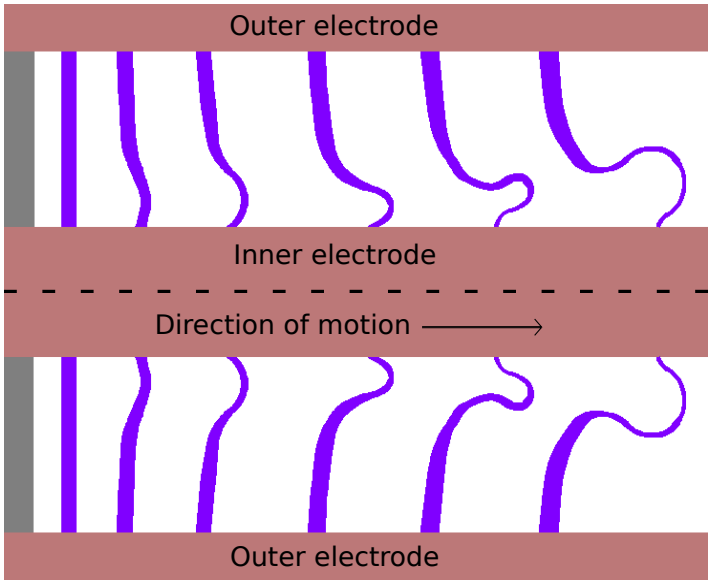

Figure 2.2: Illustration of the evolution of blow-by inside a coaxial gun. Brown shaded areas represent the electrodes, gray regions the breech insulators, purple areas the plasma, and unshaded regions empty space. Blow-by develops rightwards in the image.

entirely is very difficult. To fully avoid the onset of blow-by, the primary acceleration period of the plasma gun should be as short as possible. For coaxial guns with lower driving current than 500 kA, the acceleration period should be limited to less than a few microseconds. If this is not achievable, different approaches can be taken to increase the onset time of blow-by and extend the potential acceleration period. The onset time can be delayed by altering gas injection density, current pulse shapes, plasma temperature, and electrode geometry. Prefilled Marshall-type coaxial guns suffer the most from blow-by. Because the magnetic pressure decreases radially, mass should be concentrated near the central electrode. In the case of a $1/r^2$ initial radial density distribution, blow-by can be totally avoided because the density and pressure distributions will cancel out. This density distribution can be approached using the puffed-gas method of a Cheng-type gun[26], but it is extremely difficult to reach the ideal distribution using standard coaxial gun geometry. Time to blow-by can also be decreased by lowering driving current. Less blow-by occurs in coaxial guns operated at lower current, even if their electrodes are extended to allow them to reach the same velocities as higher-current guns. Unfortunately, longer guns have problems with secondary arcing, so there is

an inherent trade-off with this approach. Increases in plasma temperature decrease time until blow-by occurs. As devices are often designed to achieve certain plasma temperatures, however, this limitation may simply need to be designed around. Coaxial guns allow for limited control over the temperature of plasmas created during electrical breakdown. Temperature can only be controlled effectively if pre-generated plasma is inserted into the gun. The key aspect of electrode geometry which impacts blow-by is the radii of the electrodes. This occurs for two reasons. Total magnetic pressure is dependent on the inductance per unit length of the electrodes, the so-called inductance gradient. As coaxial guns are cylindrical, the inductance of a given point in the space between the electrodes depends on the radius. Thus, the ratio of the radii of the outer and inner electrodes is used to calculate the inductance gradient. Blow-by time decreases with an increase in the inductance gradient caused by an increase in the ratio between the outer and inner electrodes. Cassibry et al. suggest an upper limit of 2:1 electrode radius ratio to reduce the effects of blow-by. Increasing the total radius of both the inner and outer electrodes has the effect of increasing blow-by times. Thus, larger electrodes are desirable from a blow-by perspective. A different approach can be found with Witherspoon et al., who use an alternative "hornet" shaped geometry for reducing the effects of blow-by. Plasma is electrothermally injected between the electrodes as modeled by Cassibry. It then travels into a concave region, where the plasma is primarily compressed against the inner electrode. This allows the density distribution to approach the ideal case. The plasma then expands through a convex region towards the exit of the gun, slightly accelerating the flow. This geometry avoids blow-by, but currently is prohibitively expensive for most applications, and not necessary for devices with more measured goals[43] [45][44].

2.5 Material considerations

One of the primary attractions of coaxial plasma guns as compared to linear plasma railguns is the relatively high purity of their ejected plasma in comparison with other sources. This property has been noticed since early in their development, and maximizing purity increases the usefulness of coaxial guns[46]. There are three main sources of impurities in coaxial gun plasmas. The first is impurities already present in the gas fed into the gun. Care must be taken to acquire high-purity gas supplies, but these impurities make up only a small part of the total. The second source of impurities is from the plasma-facing insulator between the electrodes. In linear plasma railguns, erosion of the insulator material tends to be the largest source of impurities[47]. Due to the smaller plasma-facing surface area of insulators on coaxial plasma guns, this is less of a concern. Regardless, low-erosion insulators decrease impurity content in plasma ejected from coaxial guns. Along with out-gassing considerations inside high-vacuum systems, a limited variety of insulators are suitable for this purpose. The best-performing insulators have high thermal conductivity along with higher mechanical strength. Candidates for these materials include metal oxides such as alumina, metal oxide composites, some mica-based glass ceramics such as Macor, and some other advanced ceramic composites. Alumina and metal oxides produce the least amount of impurities[48][49].

The primary source of impurities in coaxial guns is ablated material eroded from the surface of the inner and outer electrodes of the plasma gun[37]. Electrode ablation and erosion occur due to a variety of causes, but the most significant is melting due to high current densities. Geometrical changes which reduce current densities also decrease electrode erosion[45]. As coaxial gun electrodes are typically constructed from metals, eroded electrode ions are likely more massive than ions eroded from insulator material or from impurities in the gas feed. Even small amounts of eroded electrode material have large impacts on the exit velocity due to their mass and their likelihood to cause restrike. The cheapest common electrode material is stainless steel, however it experiences relatively high rates of erosion. In addition,

stainless steel has a negative effect on initial and secondary breakdowns of neutral gas[42]. Of standard materials, copper alloy electrodes undergo the least erosion under high-current arcs. Pure copper can be somewhat difficult to machine, but the addition of tungsten to the alloy significantly improves machinability and may reduce erosion rates, making tungsten-copper alloys more useful electrode materials. Other additives to copper typically cause more ablation than tungsten[50][51].

Chapter 3

Design

3.1 Objectives

The coaxial plasma railgun was designed to accelerate plasma jets with electron number densities on the order 10^{16} cm$^(-3)$ up to velocities of at least 10 km/s, preferably greater than 20 km/s. These properties are considered sufficient to perform future plasma jet collision experiments. Secondary priorities included size, cost, ease of maintenance, and integration with other lab equipment. The coaxial gun was designed to be mounted on any existing and future KF-40 vacuum ports available at the Virginia Tech Center for Space Science and Engineering Research. The cost of materials and fabrication was not two exceed several thousand dollars. The design was intended to be easily maintained, cleaned, and repaired if necessary. Finally, integration with existing lab equipment was required for the coaxial gun to function. The design decisions discussed in the following chapter were made to meet these core objectives.

3.2 Experimental setup

Construction and operation of the coaxial plasma gun took place in the same facilities as prior work using the Virginia Tech linear plasma railgun[52]. The coaxial gun mounts onto a standard KF-40 flange on a 1.2 m long, 1 m diameter, 0.76 m^3 vacuum chamber. The vacuum chamber has two KF-40 ports and eight 30 cm ports which can be fitted with KF-

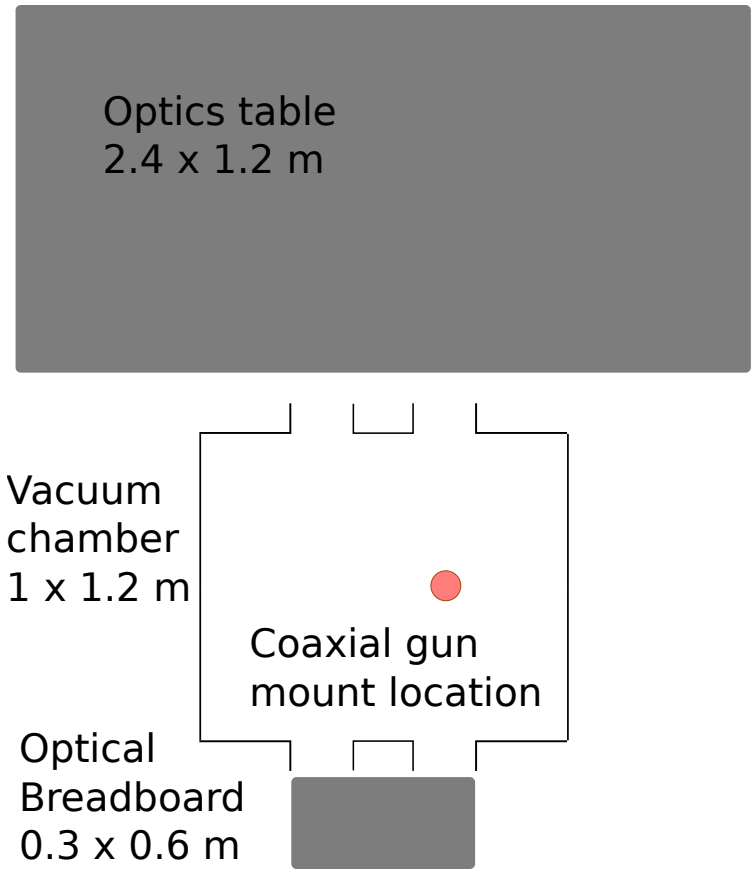

Figure 3.1: 1:23 scale top-down view of the testing environment.

40 adapters. For initial characterization testing, the gun was mounted on the top of the chamber, perpendicular to two 30 cm viewports. Diagnostics were mounted on an optical table on one side of the chamber, and an optical breadboard on the other, as shown in Figure 3.1. Specific diagnostics will be discussed in Chapter 5. The chamber reaches approximately 10^{-7} torr during normal testing. This pressure is reached by first roughing the chamber to around 5×10^{-2} torr using Trivac D40B oil sealed rotary vane dual stage vacuum pump. A Torrmaster TM500 20 inch inlet cryopump is then used to reach testing pressure.

Safety measures mirror those used for operation of the linear plasma railgun[52]. These include hardware and software interlocks which must be activated before firing, an emergency kill switch which disconnects all power supply, and a reed switch mounted to the laboratory door which does the same.

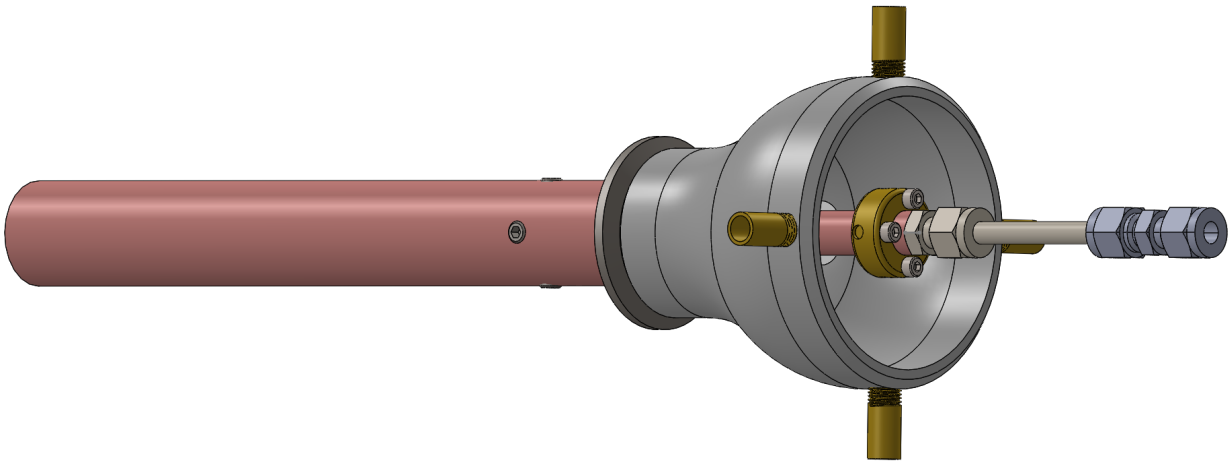

Figure 3.2: Rendering of the exterior of the coaxial gun.

3.3 Design overview

Coaxial plasma guns are more difficult to construct than linear guns of similar specifications. The coaxial configuration of the electrodes introduces more complex electrical connections, sealing points, and attachment methods. Cylindrical components can be more difficult to fabrication as well. Many parts of the coaxial gun must be pulled through each other to be removed, which rules out the use of a permanent adhesive except for in specific locations.

The final design consists of inner and outer electrodes, inner and outer power feedthroughs, three insulators, and a variety of fittings and hardware. The inner and outer electrodes are separated by a plasma-facing insulator and an internal insulator. These two insulators are attached to each other with an adhesive, and held in place with a series of set screws. The outer electrode is threaded onto a pipe nipple, the other end of which is threaded into a custom-designed KF-40 blank. The inner electrode extends through a hole in this blank. Gas is fed into the assembly through a threaded connection at the end of the inner electrode. A machined collar is attached to the inner electrode to act as an inner power feedthrough, while a concentric pipe reducer press fit to the custom blank acts as the outer power feedthrough. An external insulator sits between the outer power feedthrough and the inner electrode to

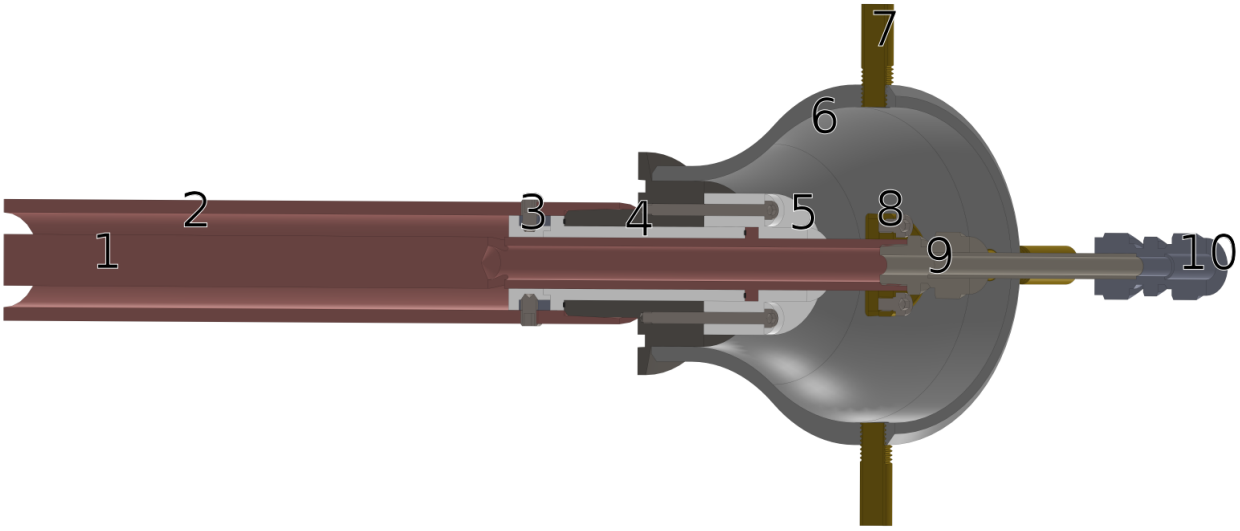

Figure 3.3: Cutaway view of the coaxial gun showing 1) the inner electrode, 2) outer electrode, 3) plasma-facing insulator, 4) internal insulator, 5) external insulator, 6) outer power feedthrough, 7) coaxial cable outer connectors, 8) coaxial cable inner connector and feedthrough collar, 9) gas puff-valve standoff, 10) gas puff-valve connection point.

prevent arcing through air. A rendering of the external view of the coaxial gun can be seen in Figure 3.2 and a cutaway view in Figure 3.3. A list of gun components can be seen in Table 3.1. The gun can be assembled and disassembled for relocation, cleaning, and replacement of damaged parts in a matter of minutes.

There are two primary sealing surfaces on the coaxial gun. The first is a face-seal joint formed by a fluoroelastomer o-ring compressed between a shoulder on the inner electrode and the upper surface of the internal insulator. Sealing force is applied to this o-ring using bolts screwed into the custom KF-40 blank. It was initially believed that a significant clamping force would be necessary to maintain this seal, but it has been shown to effectively maintain vacuum with less than half the expected force. A serious drawback of the previously existing linear railgun is the extensive use of Loctite 9492, also known as Hysol 1C vacuum epoxy, trade name Torr Seal. This heavy use of Torr Seal makes assembly and disassembly of the linear gun difficult and time-consuming. In addition to avoiding this drawback, limiting use of Torr Seal on the coaxial gun is necessary because of the more complex design. The second seal is located between the outer surface of the internal insulator and the custom blank. This

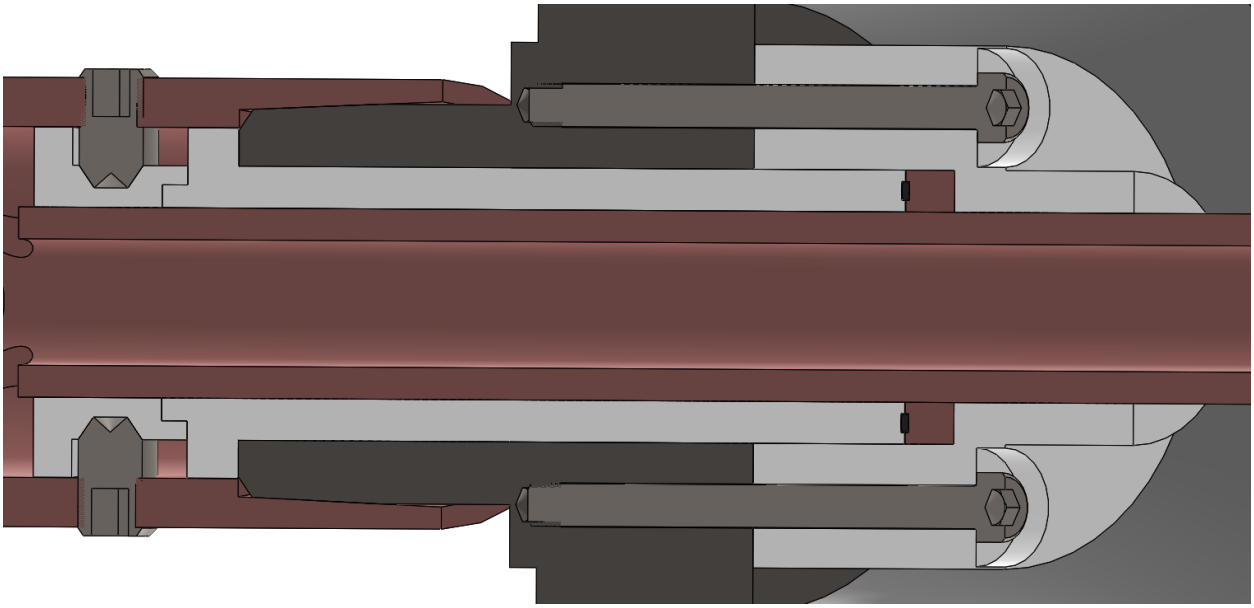

Figure 3.4: Cutaway view of the coaxial gun focusing on the triple seal location.

seal is the second point on the gun where an adhesive is used. The initial design featured an o-ring compressed between the outer electrode and the opposite end of the internal insulator, but this was not easily fabricated. Torr Seal applied around the blank-insulator interface forms the seal instead. A cutaway view focusing on the triple seal is shown in Figure 3.4

3.4 Material selection

The primary constraints on material selection in the coaxial plasma gun were material properties and budget. These traits were often in opposition to each other, severely limiting the available options for materials in the gun. Several dozen different materials were examined before the final candidates were chosen and the components manufactured. Non-ideal compromises had to be made in material choice for the final design.

Components used in all vacuum systems face two primary material property challenges. For the coaxial gun to be successful, any materials used in its design must meet the following criteria: first, they must be vacuum compatible - they must have negligible rates of outgassing

and diffusion, and must maintain their shape under high or ultra-high vacuum. Second, the materials chosen must be mechanically robust so that they can withstand assembly, operation, and disassembly. Two additional requirements were determined to be less critical. Power feedthroughs and electrodes must be capable of carrying high pulsed currents. Plasma-facing materials must be resistant to the extreme heat flux associated with plasma exposure.

Outgassing of materials occurs when the pressure of the vacuum facing a given material is lower than the vapor pressure of either the material itself, impurities in the material, or gases absorbed into the material. Metals do not tend to absorb much gas, but their oxide layers sometimes can. Problematic metals thus tend to have high vapor pressures. Some common non-metallic alloyants may also outgas significantly. Alloys containing antimony, cadmium, lead, magnesium, sulphur, or zinc should be avoided for this reason. Plastics are more problematic because they both have higher vapor pressures, and absorb more gasses. Many plastics also have high porosity. Few plastics are suitable for high or ultra-high vacuum applications. Non-porous ceramics are generally safe for use in vacuum[53]. The gun is operated using injected argon gas, and diffusion of injected gas is a negligible concern due to argon's relatively high molecular weight.

Since the coaxial gun is operated at room temperature, with high temperatures only experienced on the plasma-facing surfaces, mechanical properties for most materials are not an issue. Some materials are ruled out, such as graphite for electrodes, or certain types of weak ceramics and plastics for insulators. As these materials typically have other drawbacks, the number of acceptable materials is not significantly reduced, though this does rule out kapton. Mechanical strength is necessary, but not difficult to achieve.

Unfortunately, components made of materials which best fulfill these requirements tend to be very expensive. They are either made of expensive materials, require difficult and time-consuming fabrication processes, or both. Materials that are vacuum compatible and mechanically robust are limited to ceramics, certain metal alloys, and a very limited selection

of plastics. Metals with low melting point or thermal conductivity are ruled out for plasma-facing applications, as are all plastics. Many otherwise viable ceramics shatter under the thermal stress of plasma exposure. Current-carrying and plasma-facing material selection along with cost considerations of individual components will be discussed in the following section.

3.5 Components

3.5.1 Electrodes

The electrodes are the most important components of any railgun. On this coaxial railgun, the inner electrode is a cylindrical rod with a diameter of 1.83 cm and a length of 33.0 cm. Injected gas enters the breech of the gun through two small holes located 18.0 cm from the muzzle end of the gun. This length corresponds with the rail length of the gun. The remaining 15.0 cm connects to the inner power feedthrough and acts as the gas feedthrough for the gun. The outer electrode is 22.5 cm in length with an inner diameter of 2.33 cm and an outer diameter of 3.00 cm. Blow-by and restrike are major sources of acceleration loss in coaxial plasma guns. In this case, blow-by is unlikely, as it is operated at a very low current for a railgun, 90 kA. The gun geometry was also designed to minimize blow-by likelihood. Differences between acceleration on the surfaces of the inner and outer electrode increase with electrode radii ratio, and blow-by develops more quickly for larger ratios. Cassibry et al[45] recommend that acceleration differences greater than one order of magnitude should be avoided. This corresponds with an electrode radii ratio of 2:1. The ratio of the electrode radii for the coaxial plasma railgun is 1.81:1. Restrike is caused by high current densities Restrike rarely causes problems for railguns operated at under 100 kA, even when they are meters in length. The coaxial plasma railgun is short enough that any primary arc will have left the gun before a significant amount of current can be lost to a restrike arc, if one forms

Table 3.1: Components used in the design of the coaxial gun and the material chosen for their fabrication.

Category	Component	Material
Electrode	Inner	50% tungsten-copper
	Outer	50% tungsten-copper
Insulator	Plasma-facing	Macor
	Internal	PEEK
	External	PVC
Power feedthrough	Inner	360 brass
	Outer	304 stainless steel
	Outer connector	360 brass
Gas feedthrough	Standoff connector	Acetal (POM)
	Puff-valve adapter	304 Stainless steel

at all[37].

As they are plasma-facing and current-carrying, materials used in the electrodes must fulfill every criteria for material selection. In addition, the coaxial configuration means that the material must be machinable using a lathe. As discussed in Chapter 2, the ideal materials for both current capacity and electrode erosion are high-purity copper alloys. Table 3.2 contains an example of erosion rates for different copper alloys. Pure copper has low machinability, a significant concern on a turned piece because any internal chips or burrs may be impossible to remove. This suggests that a more machinable copper alloy should be used instead. Brass does not meet vacuum compatibility requirements and aluminum bronze suffers from high plasma ablation, as do most aluminum alloys. A 50% tungsten, 50% copper alloy was settled on for the final electrode designs. Tungsten-copper has relatively high machinability, and similar ablation rates to pure copper. Tungsten-copper is more expensive than pure copper, but the decreased machining time leads to cost savings. The completed inner electrode is shown in Figure 3.5.

Table 3.2: Electrode erosion rates of moving arcs in atmosphere with a maximum current of 250 kA [51]. Relative erosion rates are again expected to be similar for railgun electrodes. LaB_6 composites provide the best plasma erosion resistance but are not readily available.

Material	Eroded volume ($\times 10^{-3} cm^3$)
Cu	1.58
Cu + LaB_6	2.69
CuNb	1.43
CuNb + LaB_6	0.97
CuW	1.24
CuW + LaB_6	0.89
CuW + Sb	1.37

Figure 3.5: Photograph of the inner electrode. Note the holes approximately halfway along the electrode where the injected gas from the puff-valve is released into the breech of the gun. Also note the step near the right end where an o-ring forms a seal against the internal insulator. A region of lighter coloration at the far right end indicates the location of the inner power feedthrough collar.

3.5.2 Insulators

The three insulators used in the coaxial plasma gun are the plasma-facing insulator (element 3 in Figure 3.3, the internal insulator (element 4) and the external insulator (element 5). While using a single insulator for the entire assembly would be ideal from a structural perspective, The three insulators face different environments which necessitate different materials.

The plasma-facing insulator is cylindrical in shape and 1.5 cm long. It is held in place from the outside by set screws just behind the gas injection port. The top surface of the insulator forms the breech of the gun, directly interacts with the densest plasma, and is a potential arcing surface. This rules out construction from nearly all plastics. As discussed in Chapter 2, alumina or metal-oxide composite ceramics fulfill these requirements the best, as shown in Table 3.3. However, the machining downsides of these materials are even more severe than with copper. Pure alumina is nearly impossible to machine, requiring diamond-grinding over long periods of time. Instead, it is usually sintered. Sintering is expensive as it requires the manufacture of custom dies in which the sintering occurs. Thus, alumina and other sintered ceramics were not considered cost-effective. Some machinable ceramics are also available. These typically do not have the same level of desirable properties as non-machinable sintered ceramics, but are still within the required range. A boron-nitride, aluminum-nitride composite ceramic used for the linear plasma gun was passed over in favor of Macor, a primarily silica-based composite ceramic. Macor was cheaper and easier to machine.

The completed plasma-facing insulator is shown in Figure 3.6. A step on the inner surface allows it to cleanly slide onto the internal insulator. A shoulder on the internal insulator holds it in place between the plasma-facing insulator and the pipe nipple which connects the outer electrode to the power feedthrough. A thinner section extends through the custom KF-40 blank and sits against the o-ring groove on the inner electrode. The internal insulator does not face any extreme heat conditions, but it forms both vacuum seals on the coaxial

Table 3.3: Single-shot weight change of selected candidate insulator materials tested using a 160 kA linear railgun[48]. Weight is lost when insulator material is eroded. Weight losses vary between railguns, but relative differences are similar. Ceramics are superior for plasma-facing applications due to their minimal loss of material from erosion.

Material	Weight change (g/m^2)
Polycarbonate	-10.8
Glass epoxy	-26.4 – -41.8
Glass polyester	-79.4
Glass polyimide	+3.2
Macor	-11.1
Silicon nitride (sintered)	-0.7
Partially stabilized zirconia	0
Transformation toughened Alumina	+0.2
Alumina/Silicon-carbide composite	0

Figure 3.6: Photograph of the plasma-facing insulator. The breech surface is facing upwards in this photograph.

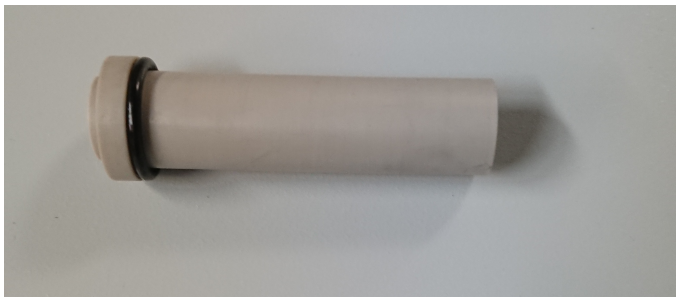

Figure 3.7: Photograph of the internal insulator. The plasma-facing insulator slides onto the left side. One sealing surface is formed about halfway down the length of the insulator using Torr seal. The second sealing uses an o-ring compressed on the flat-ended right side.

gun. It must be vacuum compatible, machinable, and Torr Seal must adhere to it. Several materials qualify such as vespel polyimide and polyether ether ketone (PEEK). These materials are comparable for this application, but PEEK was chosen for the coaxial gun due to its availability at lower prices and previous experience with its use in the linear railgun. It is shown in Figure 3.7.

The external insulator provides the clamping force which holds the o-ring seal in place. As it has no vacuum exposure, the only requirement is mechanical strength. Large forces are not necessary to maintain o-ring seals at high vacuum. PVC was chosen for its low price.

3.5.3 Power feedthrough

The power feedthrough has two sections. The inner feedthrough is very simple. Since the inner electrode extends outside of the vacuum chamber, current travels down the length of the electrode through a brass collar mounted at the back end near the gas puff-valve connection. This collar is connected to the inner conductors of RG213/U coaxial cables which are wired to the PFN.

The outer power feedthrough is more complex, as it also acts as the mounting point to the vacuum chamber. Mounting is achieved using a custom-machined KF-40 blank made of 304 stainless steel. The only difference from a standard KF-40 blank is the centered rod

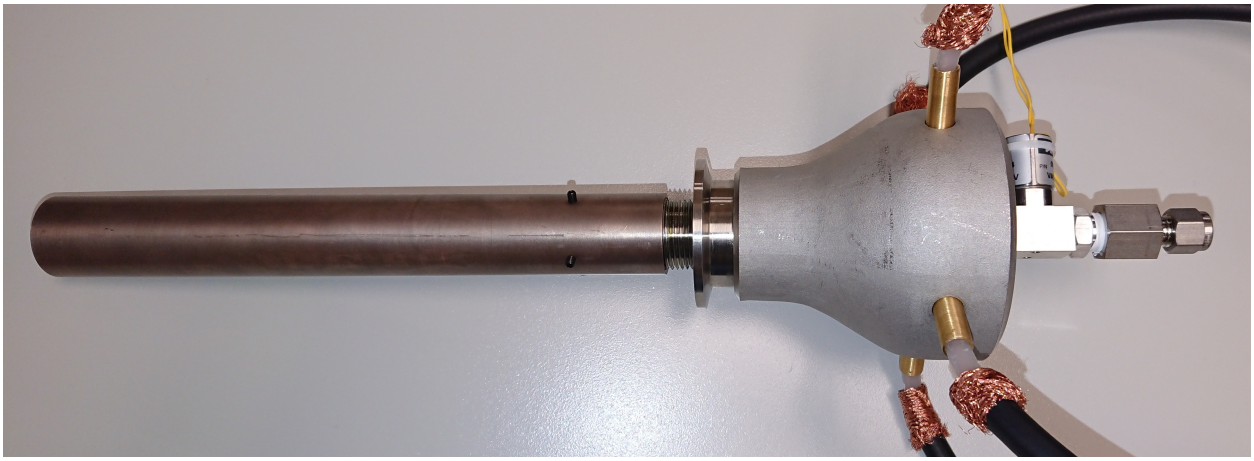

Figure 3.8: Photograph of the assembled coaxial plasma railgun. The outer power feedthrough can be seen immediately to the right of the copper-tungsten outer electrode. From left to right: first is the custom blank, followed by the pipe reducer, which connects with the coaxial cables using the brass bushings. The coaxial cables carry current from the pulse-forming network to the gun.

which extends outwards from what would be the surface of a standard blank. Four threaded fractional #4-40 holes were tapped into the top of the rod. The holes are used to bolt the external insulator in place. Current travels through the custom blank from the outer electrode and into a pipe reducer which is press-fit onto the outside of the rod. Near the top of this reducer, four brass bushings press fit in place connect to the outer conductor of the coaxial cables. A photograph of the assembled gun, including the power feedthrough, is shown in figure 3.8.

3.5.4 Gas valve

Gas-puff action is performed by a Parker Series 99 solenoid dispense valve. This valve is mounted with a series of adapters to an orifice at the back end of the inner electrode. Line pressure of argon behind the valve is maintained at 100 psi. The gas is supplied through approximately 25 feet of plastic tubing. A software-triggered LCR circuit delivers an underdamped 150 V pulse to the valve. The pulse has an approximately 2 ms pulse-width, so the valve is only open long enough to inject 4.3 ± 0.2 mg of argon. This injected

gas travels approximately 20 cm to the exit holes further down the inner electrode.

3.5.5 Pulse-forming network

An LC pulse-forming network (PFN) delivers power to the coaxial plasma gun. This PFN was originally designed for the previous linear plasma railgun, so it is sufficient, but not ideal for use with the coaxial plasma gun. A more tuned PFN would result in higher muzzle velocities. The PFN consists of two 100 μF capacitors in series and six 1.3 μF capacitors in parallel. The resulting capacitance is approximately 58 μF. They are connected together with a 6061-aluminum buswork whose geometry has been tuned to provide the desired inductance. The PFN provides a 10 to 15 μs pulse-width at a maximum of 22 kV.

Chapter 4

Characterization

4.1 Diagnostic methods

Several diagnostic methods were used to collect data for the characterization of the coaxial plasma gun. Characterization was focused on line-integrated density as inferred from interferometer measurements and velocity estimated using a photodiode. Due to the geometry of the testing chamber, the closest possible measurement point to the gun is located approximately 29.7 cm from the end of the electrodes. Data collection and analysis methods are discussed in the following sections. A diagram showing the diagnostics used during this experiment is shown in Figure 4.1

4.1.1 Rogowski Coil

Direct current measurement methods such as current shunts can change the inductance of a circuit enough to be significant for a finely-tuned PFN. Rogowski coils are an alternative measurement device which do not have to be directly integrated into a circuit. They are constructed by bending a solenoid into a toroidal shape, and passing the return wire back through the inside of the solenoid. This toroid is wrapped around a wire or other straight conductor. When the current passing through the straight conductor changes, the resulting change in the magnetic field induces a current in the Rogowski coil. For a current, $i(t)$, which is passing through a Rogowski coil with winding cross-sectional area a and winding

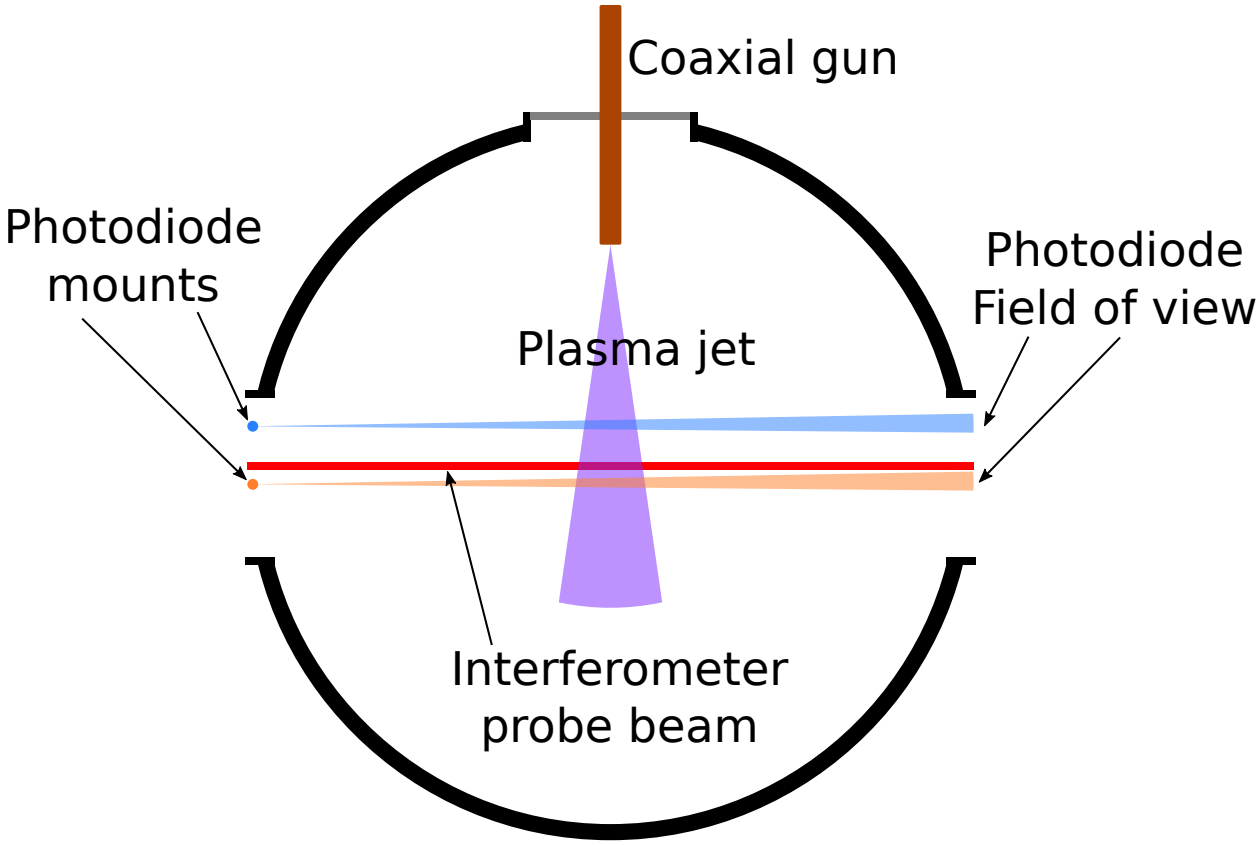

Figure 4.1: 1:10 scale cross-sectional diagram of the vacuum chamber used for testing and the positions of diagnostic equipment. The interferometer and photodiode are aimed into the chamber through glass ports on the side.

unit length, s, the voltage induced in the coil, $v(t)$ is given by the following relation[54]:

$$v(t) = \frac{\mu_0 a}{s} \frac{d}{dt} i(t) \tag{4.1}$$

where μ_0 is the magnetic permeability of free space. If the solenoid windings on the coil have a constant cross section and separation width, the change in current through the conductor of interest can be calculated from the induced voltage in the Rogowski coil. The voltage can be passed through an integrator circuit or integrated digitally to find the current in the conductor. The cross section and winding can be tuned to the expected current output to provide an induced voltage within whatever range is required for data collection. Rogowski coils can collect current data on even extremely fast pulses, their resolution depending on

the sample rate of the data acquisition system.

A Rogowski coil designed to produce an approximately 10 V induced voltage at 90 kA is placed around the inner conductors of the coaxial cables which connect to the PFN. Rogowski coil data is collected for It is used during experiments with the coaxial plasma gun to collect current data for troubleshooting, and for timing of the gas puff-valve and diagnostic equipment.

4.1.2 Interferometry

Interferometry is commonly used in plasma science to examine density and magnetic field features without directly probing a plasma. Interferometry takes advantage of changes in the refractive index of plasmas as their properties change. There are a variety of configurations, but all types of interferometers involve a reference beam and one or more probe beams. The difference in phase between the probe beam and the reference beam, $\Delta\phi$, is used to calculate the difference in the refractive index between the medium traversed by the probe beam and the reference beam. This phase difference can be seen as an interference pattern when the two beams are recombined. For this experiment, a Mach-Zehnder interferometer configuration is used to measure phase difference. A Mach-Zehnder interferometer uses two beamsplitters; one to split the probe from the reference beam, and one to recombine them. The refractive index, N, of a strongly-ionized plasma for a beam frequency ω depends on the plasma frequency, ω_p, which is itself a function of the electron density, n_e:

$$\omega_p^2 = \frac{n_e e^2}{\epsilon_0 m_e} \tag{4.2}$$

where e and m_e are the charge and mass of the electron and ϵ_0 is the dielectric permittivity of free space. N can be calculated as follows for a given beam frequency, ω:

$$N = \sqrt{1 - \frac{\omega_p^2}{\omega^2}} \tag{4.3}$$

The probe beam and the reference beam follow parallel paths through the vacuum chamber. Phase differences between the beams are related to the difference in optical path length, OPD:

$$\Delta\phi = OPD\frac{\omega}{c} \tag{4.4}$$

Optical path differences due to differences in refractive index depend on the distance travelled through each medium:

$$OPD = \int (N_1) dl_1 - \int (N_2) dl_2 \tag{4.5}$$

As the refractive index of vacuum is unity, this can be collapsed to the following:

$$OPD = \int (N - 1) dl \tag{4.6}$$

Thus, phase difference can be calculated as:

$$\Delta\phi = \int (N - 1)\frac{\omega}{c} dl \tag{4.7}$$

Putting all of the pieces together, when the phase difference is known, electron density can be found from the following integral:

$$\Delta\phi = \frac{\omega}{c} \int \left(\sqrt{1 - \frac{\frac{n_e e^2}{\epsilon_0 m_e}}{\omega^2}} - 1 \right) dl \tag{4.8}$$

For any given interferometer setup, the line-integrated electron density across the length l can thus be estimated if the phase difference between the probe and reference beam is known[55].

The beam source for the Mach-Zehnder interfereometer used in this experiment is a 632 nm Model 1122 P Lumentum 2 mW HeNe laser. An additional 80 MHz frequency is introduced to the reference beam via modulation using an IntraAction ATM-801A1 acousto-optic modulator (AOM). In this so-called heterodyne configuration, phase differences appear at the measurement device as changes in the beat frequency created when the arms of the interferometer are recombined. Changes in the refractive index will cause the beat frequency to increase or decrease relative to a calibration frequency which has no phase shift. Due to the modulation, there is no ambiguity regarding the sign of phase changes and amplitude variations have little impact on measurement. The recombined reference and probe beams are collected using a 150 MHz Thorlabs PDA10A fixed-gain detector. The resulting signal is processed with a BCL80-40-A1 lumped-element bandpass filter manufactured by MCV Microwave with a 3 dB passband from 60-100 MHz. This filters out noise and DC bias. A Pulsar IDO-04-412 IQ demodulator extracts the interference data from any remaining sinusoidal carrier frequency by splitting it into two components with a 90° phase difference according to the phase of the AOM. The 80 MHz modulation frequency is removed using a 6MHz lowpass filter. The signal is then recorded by a National Instruments PXIe-5105 60 MHz, 8-Channel, 12-Bit PXI Oscilloscope, and calculations are completed on a computer.

The electron density of plasma from the coaxial plasma gun is estimated using data collected from the interferometer described above. Average density across ten shots was estimated for the characterization PFN voltage of 7 kV.

4.1.3 Photodiode

Velocity measurements were made using a photodiode with custom amplifier circuit. Photodiodes use the photoelectric effect to convert incoming photons into an electric current: a so-called photocurrent. This photocurrent is proportional to the irradiance on the photodiode surface. For this reason photodiodes are used to measure the intensity of light sources. Because photodiodes produce photocurrents even in absolute darkness, the intensity of a light source can be measued from the difference between the measured current and a known dark photocurrent. The photocurrent is typically on the order of microvolts, so amplifier circuits are used[56].

This experiment used a single OSRAM Opto Semiconductors GmbH SFH 229 photodiode sensor with an attached amplifier circuit that saturates to 5 V. This photodiode is sensitive to light from $380 - 1100$ nm, and has a rated switching time of 10 ns. A lens is mounted to the photodiode which limits the field of view as shown in Figure 4.2. The photodiode was first placed at a position 32.8 cm from the gun muzzle. Intensity data was recorded for five shots, then the photodiode was raised to be 7.8 cm closer to the muzzle. The intensity was recorded for a further five shots at this new position. The intensities across each set of five shots were averaged, and the time of the peak average intensity found for each position. The distance between the two photodiode positions was divided by the time delay between the peak average intensity at each position to estimate velocity.

Originally, two photodiodes were intended to be used instead of one. Velocity was to be estimated by placing one photodiode at each location simultaneously. This arrangement would be superior because delay data could be collected for each shot, instead of requiring averages across multiple shots. However a fault in the second photodiode could not be fixed promptly enough for it to be used for characterization of the coaxial plasma railgun. A dual-chord interferometer could also be used to estimate velocity. This would likely be even more precise than a two-photodiode configuration, but a photodiode would still be required

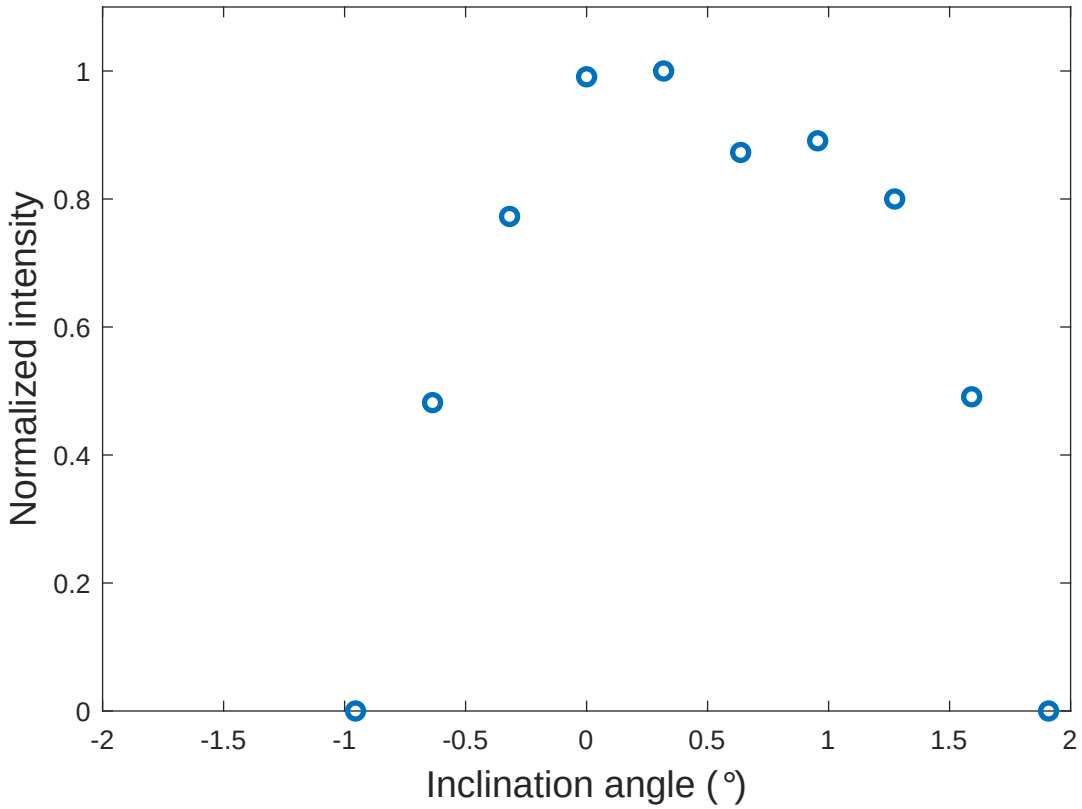

Figure 4.2: Relative intensity of a light source as measured by the photodiode circuit depending on view angle. The photodiode was mounted such that increasing view angle corresponds with closer to the muzzle of the coaxial gun, and increasing inclination.

to collect intensity data.

Chapter 5

Results

Functional operation was confirmed between 7 kV and 11 kV. To prevent potential damage to the gun, initial characterization was performed at 7 kV, the minimum test voltage possible with the existing experimental setup. Raw data can be provided upon request.

5.1 Delay timing optimization

The first step in characterizing the coaxial gun was to find the ideal timing between the triggering of the gas puff-valve and the ignition of the gun. Gas injected through the gas puff-valve takes time to travel into the breech section of the gun. In plasma railguns if the delay between the gas puff-valve and the PFN triggering is too short, then the density of gas in the breech may be too low for the gun to fire, or the mass accelerated may be too low. If the delay is too long, gas may escape the muzzle of the gun and current sheet acceleration may be slowed. In coaxial guns, the exit velocity is dependent on the density distribution of the plasma, which adds an additional challenge. Timing can also be very finely tweaked to achieve deflagration mode acceleration, although this was not examined during the characterization of this coaxial gun. The delay timing was roughly optimized by measuring average line-integrated electron densities of shots at 250 μs intervals between 1900 μs and 650 μs. The highest density was found when a 1150 μs delay was used. Commissioning and timing optimization took 36 shots.

5.2 Jet characteristics

The line-integrated electron density as measured using the interferometer is shown in Figure 5.1. The density measurements displayed in the figure are averaged across the same ten shots used to collect photodiode measurements, shots 37 to 41 and 43 to 47. A primary, dense jet can be seen with a peak at 14 μs from PFN trigger. This jet consists of two sections: a brief, but dense leading section, and an extended, lower density trailing section. Evidence of a secondary jet is visible as well, with possible third jet present near the low-end of interferometer resolution. The peak electron density of the primary jet was measured at $7.8012 \times 10^{15} \pm 3.2818 \times 10^{14}$ cm^{-2}. The mean density of the leading section of this jet was $6.0485 \times 10^{15} \pm 2.7457 \times 10^{15}$ cm^{-2}.

The presence of a primary, secondary and possible tertiary jet is also clear from photodiode data, shown in Figure 5.2. Photodiode data was collected using a single photodiode, placed at two positions spaced 7.8 cm apart. Upper position data was collected from shots 37 to 41 and lower position data was collected from shots 43 to 47. The density variation within the primary jet is also visible with an even stronger distinction than is seen in the interferometer data. The secondary jet is also more luminous than the trailing section of the primary jet. Alongside qualitative examinations, the photodiode data was also used to make an approximation of the primary jet velocity. The average velocity across ten different shots is estimated to be 130 ± 71.2 km/s. The error bounds exclude some sources of uncertainty which were difficult to quantify. A further discussion of this topic takes place in the following section.

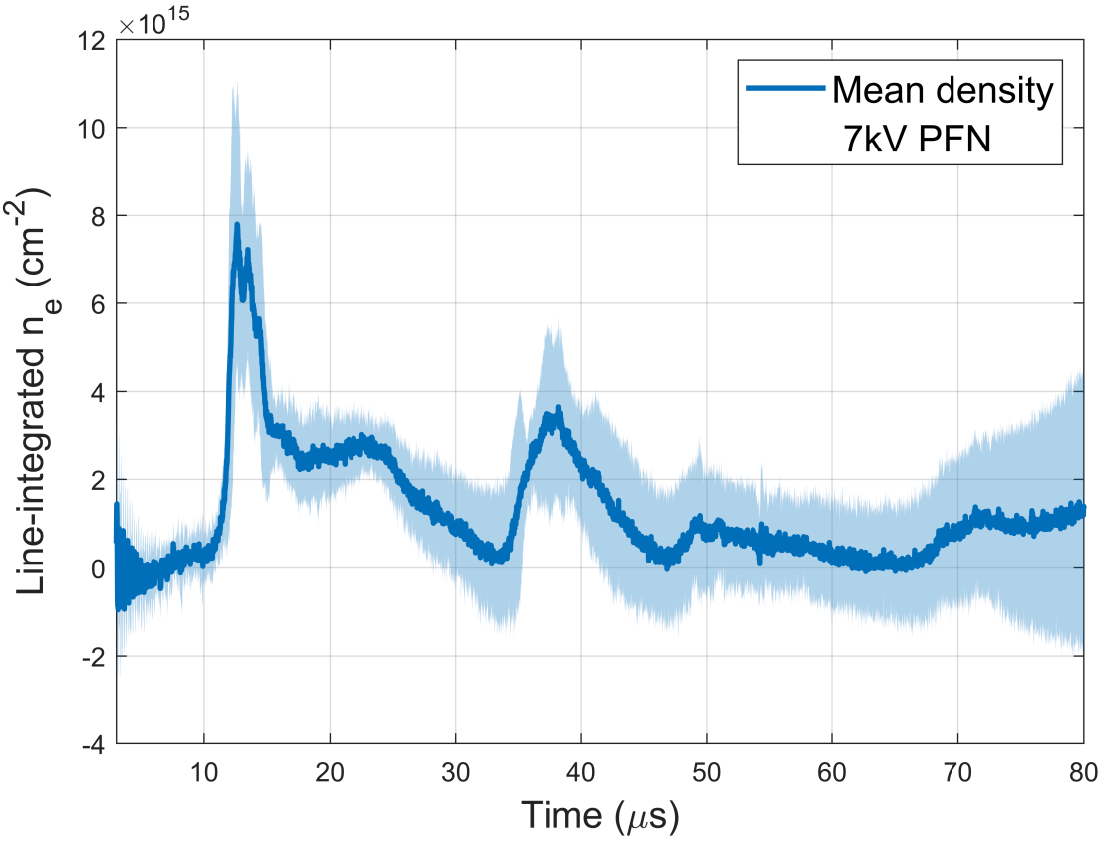

Figure 5.1: Line-integrated mean electron density measured along the interferometer chord at 29.7 cm distance from the gun muzzle taken across ten shots. Areas with lighter shading correspond to the standard deviation. Primary jet peak at 14 μs, secondary jet peak at 37 μs. Tertiary jet is partially obscured due to increased variance between shots with time.

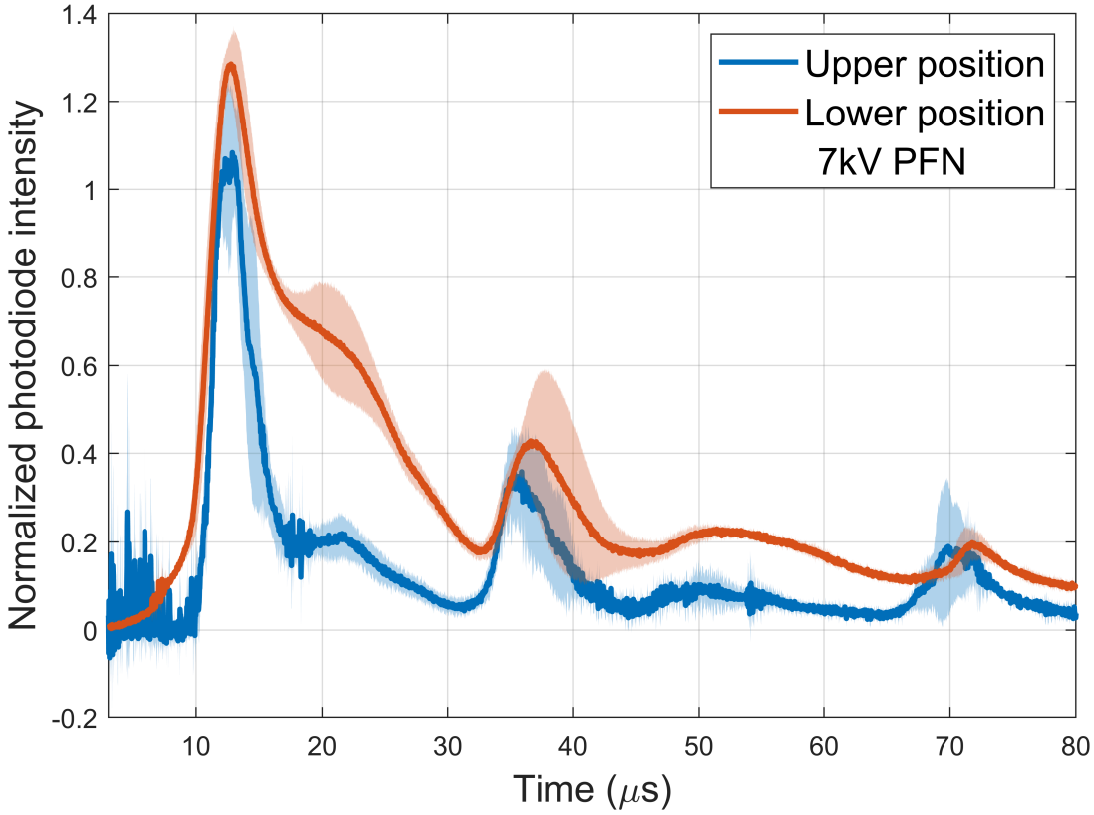

Figure 5.2: Photodiode intensity from five shots at the upper photodiode position, five at the lower position. The photodiodes were located 7.6 cm apart. Shaded regions again correspond to standard deviation. Normalization to arbitrary value. Evidence of three jets is more clear in photodiode data than the interferometer.

5.3 Discussion

The results of the characterization of the coaxial plasma gun show that it functions within the desired regime, but there is significant uncertainty about some results. Refer to Table 5.1 for key results. Phase shift measurements taken using the interferometer, and the density estimates inferred from them are likely accurate. This measurement technique has been used successfully for years at Virginia Tech[57][52] and consistently provides high-quality results. The density estimates show strong consistency between shots, with a standard deviation of less than 5% across ten shots for the peak density. The mean density across shots is less consistent, but this can be caused by even small variations in jet length and velocity. These densities on the order of $10^{15} - 10^{16}$ cm^{-3} are high enough to perform jet collision experiments.

Larger issues are present in the velocity measurements. Velocities of over 100 km/s seem to be infeasibly high given the $\approx$ 10 km/s velocities seen from the linear railgun using the same PFN. Certainly it is not possible that all of the gas injected through the puff-valve could be accelerated to this velocity. One explanation is that only a small proportion of the injected gas is actually accelerated. To check this hypothesis, a very rough approximation of the mass of plasma in the primary jet, where peak velocities occur, was made. The plasma jet was assumed to be cylindrical in shape. Jet length was approximated by multiplying the full width at half maximum of time in the interferometer trace by the average velocity as measured by the photodiode. From the width and length estimates, it was possible to estimate the approximate volume of a jet.

Full electron number density was estimated from the line-integrated density using the jet width. The mean ionization of the jet is unknown, but prior work suggests that it is likely close to unity[58][59][60], but may be as high as 2[52]. This results in ion densities between the same or half that of the electron density. By assuming the jets consist entirely of argon, a mass density can be derived from the ion density, and then using the volume of a jet, an

Table 5.1: Summary of the characteristics of the primary jet. Line-integrated electron density is inferred from interferometry and error is calculated as the standard deviation across coaxial gun shots. Velocity is estimated from photodiode measurements and error calculated from measurement error combined with standard deviation across shots. The mass of gas injected by the valve is measured using a pressure sensor with known measurement uncertainty. Jet mass is derived from both velocity and electron density. Jet mass error incorporates error from velocity measurement as well as standard deviations of both interferometer and photodiode data.

Property	Value	Error	Unit	Error (%)
$n_{e,peak}dl$	7.8012×10^{15}	3.2818×10^{14}	cm^{-2}	4.2067
$n_{e,mean}dl$	6.0485×10^{15}	2.7457×10^{15}	cm^{-2}	45.395
V_{jet}	130.1	71.2	km/s	54.727
m_{valve}	4.3	0.2	mg	4.6512
m_{jet}	0.137	0.121	mg	88.321

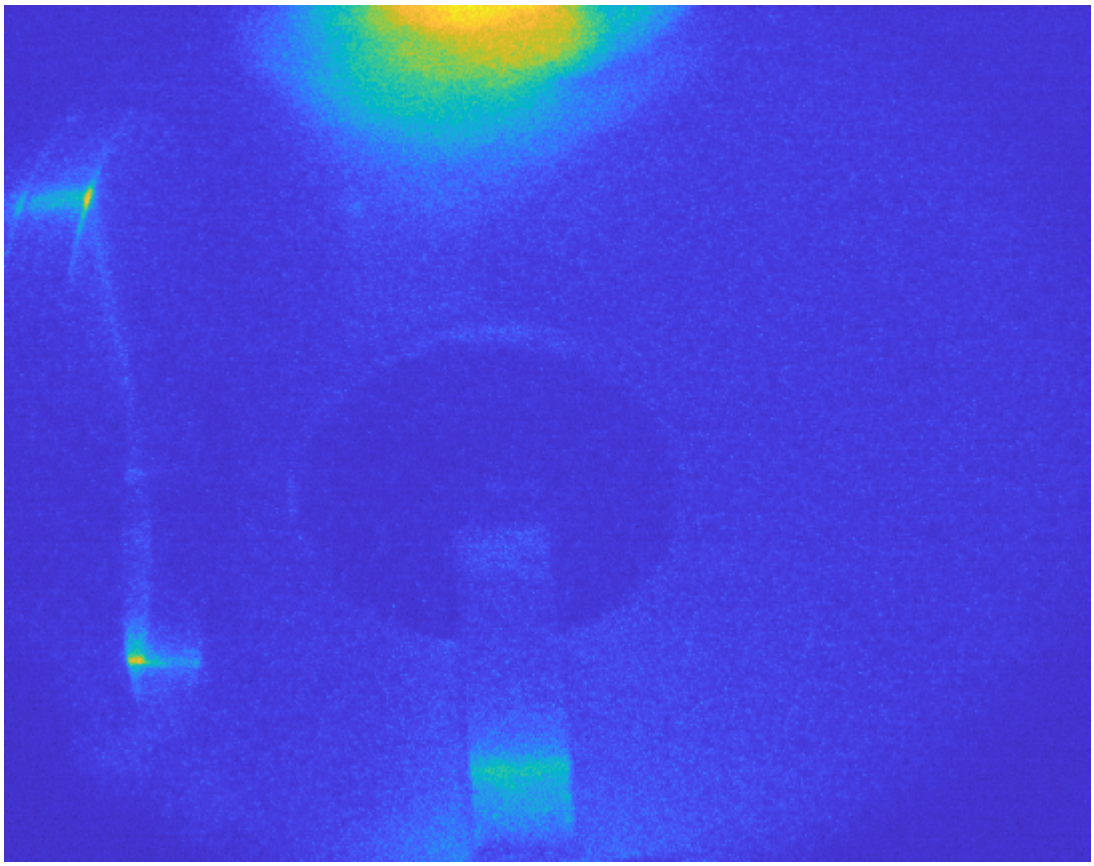

Figure 5.3: Short-exposure photograph of the leading edge of the jet which was used to calculate the width of the plasma jet. The image is logarithmically scaled with blue as least intense and yellow as most intense.

approximation of jet mass found. Using these parameters, the mass of the primary jet is estimated to be 0.137 ± 0.121 mg, between 0.4% and 6.3% of the ≈ 4.3 mg of gas injected into the gun. This jet mass is on the same order of magnitude as the mass of jets from the linear railgun calculated using the same method. To double-check the jet mass estimation, a snowplow prediction of jet velocity was made using the whole range of possible accelerated jet mass values. Figure 5.4 shows the predicted velocities of possible jet masses from this method.

If the method is accurate, jet velocities consistent with the lower range of measured velocity are possible. Jets with mass of less than 0.68% of the injected mass should be able to achieve these velocities. However, velocities of this magnitude would result in jet lengths in excess of 20 cm, compared to the ≈ 2 cm jets from the linear gun[52]. While it is possible that jets from the coaxial gun are longer due to the geometrical differences between the two guns, it should be remembered that coaxial gun jets are disk-shaped. Jets of this length are unlikely.

An extremely rough estimation for the lowest possible bound of velocity can be made using the time delay between the triggering of the PFN and the peak in line-integrated density measured using the interferometer. Plasma jets must leave the muzzle of the gun some amount of time after the PFN is triggered. If the exit timing was known, it could be subtracted from the timing of the peak line-integrated density to find the flight time of the jet between the muzzle and the interferometer. This velocity estimate would totally avoid using the imprecise photodiode data. Even if the exit timing is not known, the absolute earliest possible timing occurs the moment the PFN is triggered. Thus, to estimate a lower bound on jet velocity, it is assumed that the leading edge of the first jet exits the muzzle of the gun at the PFN triggering time. Using an average of all ten test shots, the lower velocity bound estimated from this method is ≈ 20 km/s at 7 kV. This minimum velocity still meets the target of $10 - 20\ km/s$.

Velocity measurement issues could be caused by the use of photodiodes to collect velocity

measurement data. Photodiode data for this experiment was collected by moving the photodiode between different positions across multiple shots. It is possible that this distance was too short for the time differences between the positions to overcome intershot variability. The photodiode used a custom integrator circuit, and that may have contributed to the large uncertainty surrounding the velocity calculation. Despite these shortcomings in the velocity measurement, it can still be confidently stated that velocities at tens of kilometers per second were achieved.

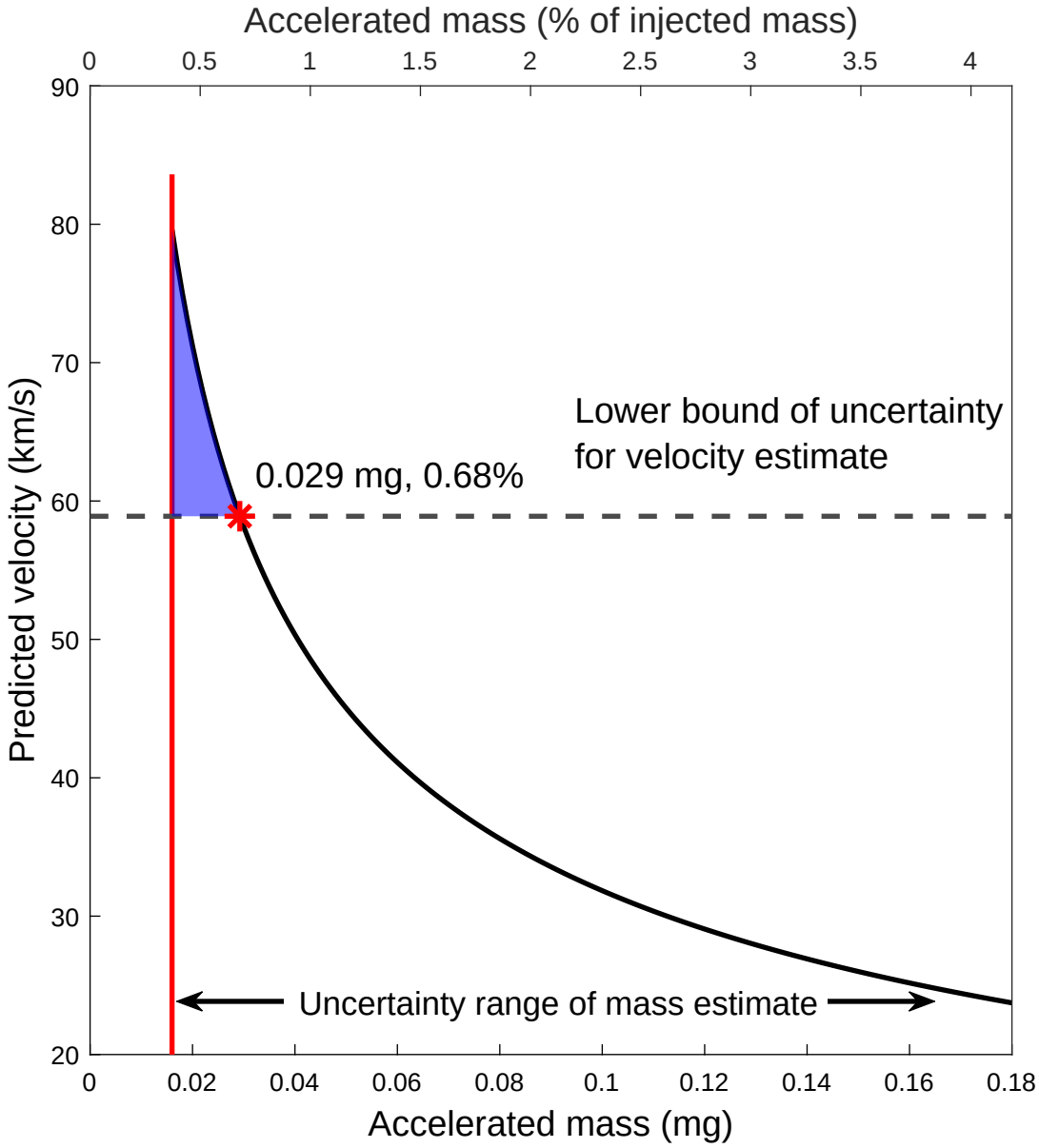

Figure 5.4: Velocity predicted by naive snowplow approximation across the whole range of possible jet mass values. All velocities above the dashed line are within the uncertainty bound of estimated velocity, 58.9 km/s. The blue region shows the space of possible masses within this allowed region. It extends from the lower bound of uncertainty for the mass estimation at 0.016 mg up to an upper limit of 0.029 mg.

Chapter 6

Conclusions

This thesis describes the research background, design, and characterization of a small, low-power coaxial plasma railgun for future use in plasma jet collision experiments. Close attention is paid to specific design decisions including material choice, component selection, and necessary accessory equipment. A description of the methods used to characterize the gun is provided. It is hoped that these descriptions will be useful for future researchers building their own coaxial guns.

6.1 Research conclusions

Although the characterization of the coaxial gun plasma was not extensive, it was sufficient to determine that the gun is functional. Plasma jets are detected via multiple methods at all test potentials from 7 kV to 11 kV. Line-integrated electron densities within the desired range are measured even at the lowest possible potentials. Jet properties at 7 kV are consistent and repeatable. However, the photodiode measurement method for velocity was not sufficient to collect precise data. While strong conclusions are harder to come to regarding the velocity of jets, it is very likely that they are in the range of tens of kilometers per second and probable that they are in excess of the velocities achieved using the linear railgun. No visible damage to the electrodes or the insulators during the characterization testing was observed, though this may be due to the chosen characterization test voltage. This may point to high purity plasma. Work on the systems shared between the new coaxial gun and the existing linear

gun has ensured interoperability between the two, and has also simplified the integration of future additional devices.

6.2 Contributions

The coaxial plasma railgun developed in this thesis uses a simple design which is expected to be cost-effective compared to other guns operating in similar regimes. The compactness and portability of the gun presented unique challenges during the design process. The in-depth description provided of this process is intended to inform future designers of small-scale coaxial guns. Finally, it is hoped that the challenges with diagnostics faced during the characterization of the gun can be avoided using the information reported here.

6.3 Improvements and future work

While the present design iteration functioned well enough for characterization, design changes should be made before intensive testing begins. There are several issues with the electrical connections. The outer power feedthrough operates well, but arcing occurs between the components of the inner power feedthrough at higher potentials. The brass collar around the inner electrode should be redesigned to eliminate this arcing. Additionally, disconnecting the gun from the PFN requires inconvenient soldering; an improved connection should be created which does not. To reduce assembly difficulties, the adhesive seal between the custom blank and the internal insulator should be replaced with an o-ring face seal. This would entirely eliminate the use of Torr seal in the coaxial gun.

Additional testing is necessary to characterize the gun to the same degree as other laboratory plasma sources at the Virginia Tech Center for Space Science and Engineering Research. Gas puff-valve timings should be explored more comprehensively to ensure that the ideal timing

is used. Electron density measurements should be taken at several different distances from the muzzle of the gun to determine jet cohesiveness. This data should also be used to improve velocity estimates of the primary jet and generate estimates for the secondary and tertiary jet. High-speed camera images of the jets should be utilized to examine the structure of these jets and how they change across space. Comprehensive spectrometer data should be collected to determine jet electron temperature and mach number. Spectrometer data should also be used in conjunction with ion gauge pressure measurements to investigate jet composition. This can be combined with an examination of the electrodes for damage after further testing.

Beyond the immediate future, the coaxial gun can be turned to its primary purpose of jet collision research in conjunction with the linear railgun. In the long term, this will require the construction of an additional PFN so that both railguns can be operated simultaneously. With a well-designed PFN and careful tuning of gas injection, the deflagration acceleration mode can be achieved, allowing the jets from the gun to reach much higher velocities. If properly maintained, the coaxial plasma railgun may be a useful tool for several thousand shots, potentially years of experimenting, before it needs to be replaced.

Bibliography

[1] C. Allardice, E. R. Trapnell, E. Fermi, L. Fermi, and R. C. Williams, *The First Reactor, 40th Anniversary (rev.)* Dec. 1982.

[2] *United states nuclear tests: July 1945 through september 1992*, Oct. 2015.

[3] D. Eisenhower, *Atoms for peace*, Dec. 8, 1953.

[4] J. A. Phillips, "Magnetic fusion," *Los Alamos Science*, vol. 4, no. 7, pp. 64–67, 1983.

[5] D. Fischer, *History of the International Atomic Energy Agency: the first forty years.* IAEA, 1997.

[6] G. Mank and A. Aqrawi, *Fifty years of magnetic confinement research - a retrospective*, 2008.

[7] S. Eklund, "Assessment of the second conference," *International Atomic Energy Agency Bulletin*, vol. 6, no. 3, pp. 5–6, Aug. 1964.

[8] *Proceedings of the Second United Nations International Conference on the Peaceful Uses of Atomic Energy: held in Geneva, 1 Sept. - 13 Sept. 1958*, vol. 31, United Nations, 1958.

[9] H. Alfven, "Magnetohydrodynamics and the thermonuclear problem," in *Proceedings of the Second United Nations International Conference on the Peaceful Uses of Atomic Energy: held in Geneva, 1 Sept. - 13 Sept. 1958*, vol. 31, United Nations, 1958, pp. 3–5.

[10] J. Marshall, "Acceleration of plasma into vacuum," in *Proceedings of the Second United Nations International Conference on the Peaceful Uses of Atomic Energy: held in Geneva, 1 Sept. - 13 Sept. 1958*, vol. 31, United Nations, 1958, pp. 341–347.

[11] J. Marshall, "Performance of a hydromagnetic plasma gun," *Physics of Fluids*, vol. 3, no. 1, pp. 134–135, 1960.

[12] J. Marshall, "Methods and means for obtaining hydromagnetically accelerated plasma jet," Granted Patent US 2961559 A, Nov. 22, 1960.

[13] H. Alfven, L. Lindberg, and P. Mitlid, "Experiments with plasma rings," *Journal of Nuclear Energy*, vol. 1, no. 3, pp. 116–120, 1960.

[14] T. Kikuta, T. Uchino, N. Akao, Y. Akahoshi, and T. Koura, *Development of micro-particles accelerator with pulse formation*, Proceedings of the 2015 Hypervelocity Impact Symposium (HVIS 2015), 2015. DOI: https://doi.org/10.1016/j.proeng.2015.04.048. [Online]. Available: https://creativecommons.org/licenses/by-nc-nd/4.0/.

[15] D. C. Hagerman and J. E. Osher, "Injection and trapping of a beta = 1 plasma into a cusped magnetic field," *Physics of Fluids*, vol. 4, no. 7, pp. 905–911, 1961.

[16] N. N. Brevnov and A. I. Matulis, "Passage of a plasma burst through a magnetic mirror machine," *Atomic Energy*, vol. 14, no. 4, pp. 359–363, 1964.

[17] E. M. Little, J. Marshall, W. E. Quinn, and T. F. Stratton, "Injected magnetic compression experiment," *Physics of Fluids*, vol. 4, no. 12, pp. 1570–1571, 1961.

[18] D. W. Koopman, "Performance studies with an electrically driven shock tube," *Physics of Fluids*, vol. 7, no. 10, pp. 1651–1657, 1964.

[19] R. G. Jahn, *Physics of Electric Propulsion*, first. New York: McGraw Hill, Jan. 1968.

[20] M. N. Rosenbluth, "Infinite conductivity theory of the pinch," Los Alamos Scientific Laboratory, Los Alamos, NM, Tech. Rep. LA-1850, Sep. 1954.

[21] P. J. Hart, "Modified snowplow model for coaxial plasma accelerators," *Journal of Applied Physics*, vol. 35, no. 12, pp. 3425–3431, 1964.

[22] P. J. Hart, "Plasma acceleration with coaxial electrodes," *Physics of Fluids*, vol. 5, no. 1, pp. 38–47, 1962.

[23] D. Petrov, N. Filippov, T. Filippova, and V. Khrabrov, "Powerful pulsed gas discharges in chambers with conducting walls," *Plasma Physics and the Problem of Controlled Thermonuclear Reactions*, vol. 4, p. 198, 1961.

[24] J. W. Mather, "Formation of a high-density deuterium plasma focus," *Physics of Fluids*, vol. 8, no. 2, pp. 366–377, 1965.

[25] D. L. Willenborg and C. D. Hendricks, "Design and construction of a dense plasma focus device," University of Illinois Urbana, Urbana, IL, Technical Report 2-76, Oct. 1976.

[26] D. Y. Cheng, "Plasma deflagration and the properties of a coaxial plasma deflagration gun," *Nuclear Fusion*, vol. 10, no. 3, pp. 305–317, 1970.

[27] D. Y. Cheng, "Application of a deflagration plasma gun as a space propulsion thruster," *AIAA Journal*, vol. 9, no. 9, pp. 1681–1685, 1971.

[28] W. C. Turner, G. C. Goldenbaum, E. H. A. Granneman, J. H. Hammer, C. W. Hartman, D. S. Prono, and J. Taska, "Investigations of the magnetic structure and the decay of a plasma-gun-generated compact torus," *Physics of Fluids*, vol. 26, no. 7, pp. 1965–1986, 1983.

[29] J. H. Hammer, C. W. Hartman, J. L. Eddleman, and H. S. McLean, "Experimental demonstration of acceleration and focusing of magnetically confined plasma rings.," *Physical Review Letters*, vol. 61, no. 25, pp. 2843–2846, 1988.

[30] K. F. Schoenberg, R. A. Gerwin, R. W. Moses, J. T. Scheuer, and H. P. Wagner, "Magnetohydrodynamic flow physics of magnetically nozzled plasma accelerators with applications to advanced manufacturing," *Physics of Plasmas*, vol. 5, no. 5, pp. 2090–2104, 1998.

[31] U. Shumlak, R. P. Golingo, B. A. Nelson, and D. J. D. Hartog, "Evidence of stabilization in the z-pinch.," *Physical Review Letters*, vol. 87, no. 20, p. 205 005, 2001.

[32] U. Shumlak, J. M. Blakely, B.-J. Chan, R. P. Golingo, S. D. Knecht, B. A. Nelson, R. J. Oberto, M. R. Sybouts, G. V. Vogman, and D. J. D. Hartog, "Stabilization in the zap flow z-pinch," *Journal of Fusion Energy*, vol. 28, no. 2, pp. 208–211, 2008.

[33] U. Shumlak, "Z-pinch fusion," *Journal of Applied Physics*, vol. 127, no. 20, p. 200 901, 2020.

[34] F. Conti, J. C. Valenzuela, N. Aybar, F. J. Wessel, M. P. Ross, J. Narkis, H. U. Rahman, E. Ruskov, and F. N. Beg, "Characterization of a liner-on-target gas injector for staged z-pinch experiments," *IEEE Transactions on Plasma Science*, vol. 46, no. 11, pp. 3855–3863, 2018.

[35] J. Cikhardt, D. Klir, A. V. Shishlov, V. A. Kokshenev, K. Rezac, R. K. Cherdizov, G. N. Dudkin, F. I. Fursov, J. Kravarik, P. Kubes, N. E. Kurmaev, V. Munzar, J. Novotny, N. A. Ratakhin, K. Turek, and V. A. Varlachev, "Neutron fluence distribution in experiments with 3 ma deuterium gas-puff z-pinch," *Physics of Plasmas*, vol. 27, no. 7, p. 72 705, 2020.

[36] L. Lindberg and C. T. Jacobsen, "Studies of plasma expelled from a coaxial plasma gun," *Physics of Fluids*, vol. 7, no. 11, 1964.

[37] J. Parker, "Why plasma armature railguns don't work (and what can be done about it)," *IEEE Transactions on Magnetics*, vol. 25, no. 1, pp. 418–424, 1989.

[38] J. Batteh, "Review of armature research (railguns)," *IEEE Transactions on Magnetics*, vol. 27, no. 1, pp. 224–227, 1991.

[39] A. Yamori, M. Kohno, and N. Kawashima, "Secondary arc dynamics in a railgun bore," *IEEE Transactions on Magnetics*, vol. 35, no. 1, pp. 452–456, 1999.

[40] R. Karhi, J. Mankowski, J. Dickens, M. Kristiansen, and D. Wetz, "Secondary arc formation within a distributed energy railgun," *IEEE Transactions on Plasma Science*, vol. 36, no. 5, pp. 2738–2746, 2008.

[41] L. C. Burkhardt and R. H. Lovberg, "Current sheet in a coaxial plasma gun," *Physics of Fluids*, vol. 5, no. 3, pp. 341–347, 1962.

[42] T. J. Gooding, B. R. Hayworth, and R. H. Lovberg, "Instabilities in a coaxial plasma gun," *AIAA Journal*, vol. 1, no. 6, pp. 1289–1292, 1963.

[43] K. Baker, D. Hwang, R. Evans, R. Horton, H. McLean, S. Terry, S. Howard, and C. DiCaprio, "Compact toroid dynamics in the compact toroid injection experiment," *Nuclear Fusion*, vol. 42, no. 1, pp. 94–99, 2002.

[44] F. D. Witherspoon, A. Case, S. J. Messer, R. Bomgardner, M. W. Phillips, S. Brockington, and R. Elton, "A contoured gap coaxial plasma gun with injected plasma armature," *Review of Scientific Instruments*, vol. 80, no. 8, 083506-083506-15, pp. 083506-083506–15, Aug. 2009. DOI: 10.1063/1.3202136.

[45] J. T. Cassibry, Y. C. F. Thio, and S. T. Wu, "Two-dimensional axisymmetric magnetohydrodynamic analysis of blow-by in a coaxial plasma accelerator," *Physics of Plasmas*, vol. 13, no. 5, p. 53 101, 2006.

[46] H. P. Eubank, "Impurity content of plasma produced by a coaxial plasma gun," *Physics of Fluids*, vol. 6, no. 10, pp. 1522–1524, 1963.

[47] J. V. Parker, W. M. Parsons, C. E. Cummings, and W. E. Fox, "Performance loss due to wall ablation in plasma armature railguns," in *18th Fluid Dynamics and Plasmadynamics and Lasers Conference*, 1985.

[48] S. Rosenwasser and R. Stevenson, "Selection and evaluation of insulator materials for high performance railgun bores," *IEEE Transactions on Magnetics*, vol. 22, no. 6, pp. 1722–1729, 1986.

[49] T. Engel and M. Kristiansen, "Mechanisms and predictors of insulator degradation and erosion produced by pulsed high-current surface discharges," *IEEE Transactions on Plasma Science*, vol. 37, no. 9, pp. 1863–1870, 2009.

[50] A. L. Donaldson, M. O. Hagler, M. Kristiansen, G. Jackson, and L. Hatfield, "Electrode erosion phenomena in a high-energy pulsed discharge," *IEEE Transactions on Plasma Science*, vol. 12, no. 1, pp. 28–38, 1984.

[51] F. Lehr and M. Kristiansen, "Electrode erosion from high current moving arcs," *IEEE Transactions on Plasma Science*, vol. 17, no. 5, pp. 811–817, 1989.

[52] M. K. Schneider, A. I. Mohammed, and C. S. Adams, "Characterization of plasma jets driven by a small linear railgun," *Plasma Sources Science and Technology*, vol. 29, no. 4, p. 045 013, Apr. 2020. DOI: 10.1088/1361-6595/ab7cc0.

[53] G. L. Weissler and R. W. Carlson, Eds., *Vacuum physics and technology*, English, 1st, ser. Methods of experimental physics. New York: Academic Press, 1979, vol. 14.

[54] M. Samimi, A. Mahari, M. A. Farahnakian, and H. Mohseni, "The rogowski coil principles and applications: A review," *IEEE Sensors Journal*, vol. 15, pp. 651–658, 2015.

[55] I. H. Hutchinson, *Principles of plasma diagnostics*, eng, 2nd. New York: Cambridge University Press, 2005, OCLC: 633694032, ISBN: 9780521675741.

[56] J. Cox, *Fundamentals of Linear Electronics: Integrated and Discrete*. Delmar Thomson Learning, 2002, ISBN: 9780766830189.

[57] M. Schneider, C. Adams, M. Popescu, J. Korsness, and M. Sherburne, "Characterization of a small railgun-based plasma jet source," in *APS Division of Plasma Physics Meeting Abstracts*, ser. APS Meeting Abstracts, vol. 2016, Oct. 2016, CP10.145.

[58] E. C. Merritt, A. L. Moser, S. C. Hsu, J. Loverich, and M. A. Gilmore, "Experimental characterization of the stagnation layer between two obliquely merging supersonic plasma jets," *Physical Review Letters*, vol. 111, no. 8, p. 85 003, 2013.

[59] E. C. Merritt, A. L. Moser, S. C. Hsu, C. S. Adams, J. P. Dunn, A. M. Holgado, and M. A. Gilmore, "Experimental evidence for collisional shock formation via two obliquely merging supersonic plasma jets," *Physics of Plasmas*, vol. 21, no. 5, p. 55 703, 2014.

[60] A. L. Moser and S. C. Hsu, "Experimental characterization of a transition from collisionless to collisional interaction between head-on-merging supersonic plasma jetsa)," *Physics of Plasmas*, vol. 22, no. 5, p. 55 707, 2015.